Paramagnetic Spin Pumping

Y. Shiomi[1] and E. Saitoh[1,2,3,4]
[1]Institute for Materials Research, Tohoku University, Sendai 980-8577, Japan
[2]WPI Advanced Institute for Materials Research, Tohoku University, Sendai 980-8577, Japan
[3]CREST, Japan Science and Technology Agency, Tokyo 102-0076, Japan
[4]Advanced Science Research Center, Japan Atomic Energy Agency, Tokai 319-1195, Japan
(Received 25 August 2014; revised manuscript received 24 October 2014; published 23 December 2014)

We have demonstrated spin pumping from a paramagnetic state of an insulator La_2NiMnO_6 into a Pt film. Single-crystalline films of La_2NiMnO_6 which exhibit a ferromagnetic order at $T_C \approx 270$ K were grown by pulsed laser deposition. The inverse spin Hall voltage induced by spin-current injection has been observed in the Pt layer not only in the ferromagnetic phase of La_2NiMnO_6, but also in a wide temperature range above T_C. The efficient spin pumping in the paramagnetic phase is ascribable to ferromagnetic correlation, not to ferromagnetic order.

DOI: 10.1103/PhysRevLett.113.266602 PACS numbers: 72.25.Pn, 72.25.Mk, 75.47.Lx, 75.76.+j

A spin current in nonmagnetic metals consists of electrons with opposite spins moving in opposite directions. This spin flow which does not accompany a net charge flow, called a pure spin current, is a key ingredient in spintronics devices [1]. A pure spin current can be detected electrically by the inverse spin Hall effect (ISHE) using metals with strong spin-orbit interaction, such as Pt. In the ISHE, electrons with opposite spins are scattered into different directions by the spin-orbit interaction, as shown in Fig. 1(a). Then, the inverse spin Hall voltage, V, arises along the direction parallel to $j_s \times \sigma$, where j_s and σ are the spatial direction and the spin-polarization direction of the spin current, respectively [Fig. 1(a)].

Spin pumping is a powerful tool to generate pure spin currents; when a magnetization precession motion is induced in a magnet, e.g., by ferromagnetic resonance (FMR), a spin current is injected into an adjacent nonmagnetic metal. During the precessional motion of magnetization, the spin angular momentum in the magnet is transferred across the interface to an adjacent metal via the spin exchange at the interface, as shown in Fig. 1(b). The spin pumping has been studied using FMR so far in ferri- or ferromagnet|paramagnetic-metal hybrid structures [2–14]. Pure spin currents produced by spin pumping were first observed by use of the ISHE in Ni-Fe|Pt double layers [2–7]. Recently, the spin pumping from a ferrimagnetic insulator $Y_3Fe_5O_{12}$ to a neighboring Pt film was discovered [9]. Spin pumping from magnetic insulators, which does not accompany spin-polarized electric currents across the interface [10], created new interest in the spintronics field from the viewpoints of applications and also of the science of spin currents [11–16].

In the present study, we have developed a new insulator for spin pumping: an oxide insulator La_2NiMnO_6 whose Curie temperature, T_C, is close to room temperature. Using La_2NiMnO_6|Pt devices, we have investigated spin pumping in the temperature range from 200 to 350 K. Below T_C, the spin current generated from La_2NiMnO_6 by FMR spin pumping is observed in an attached Pt layer via the ISHE. Furthermore, clearly, the spin-current signal appears also at *paramagnetic* resonance in La_2NiMnO_6 even far above room temperature, although La_2NiMnO_6 is in the paramagnetic state and it has no long-range spontaneous magnetization; the ISHE signal is observed in the Pt layer in a wide temperature range up to 350 K. This result is the evidence of spin pumping without ferromagnetic order.

La_2NiMnO_6 films were grown on (001) $SrTiO_3$ (STO) substrates by the pulsed laser deposition technique. Polycrystalline targets were ablated with a KrF excimer

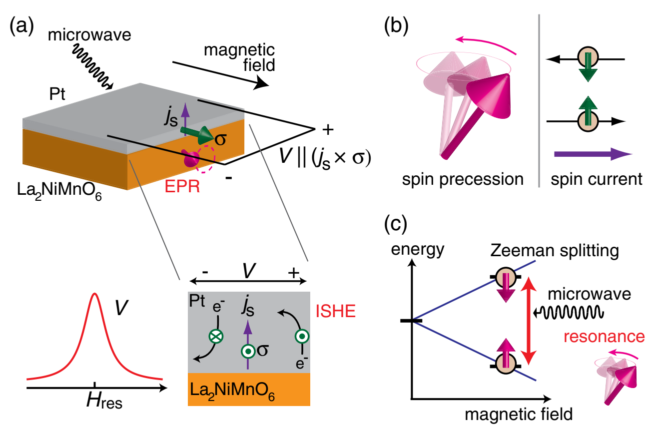

FIG. 1 (color online). (a) A schematic illustration of the inverse spin Hall effect induced by spin pumping in La_2NiMnO_6|Pt structures. (b) A schematic illustration of spin pumping. Spin precession induces a pure spin current in the adjacent layer. (c) A schematic illustration of electron paramagnetic resonance (EPR). In the presence of H, energy levels of parallel-spin and antiparallel-spin states are separated: the Zeeman effect. When the microwave frequency (f) is equal to the Zeeman energy splitting ($2\pi f = \gamma H$), electron spins precess resonantly.

 © 2014 American Physical Society

laser light ($\lambda = 248$ nm) with a repetition rate of 2 Hz. During the deposition, STO substrates were kept at 800 °C and pure oxygen gas of 0.3 torr was continuously supplied into the growth chamber. After the thin-film growth, the films were annealed at 800 °C in 400 torr oxygen gas for 1 hour, then cooled down to room temperature at the rate of 15 °C/ min. The crystal structures of the films were evaluated by reflection high energy electron diffraction (RHEED) and x-ray diffraction using Cu $K\alpha$ radiation. Clear streaks from La_2NiMnO_6 films were observed in RHEED patterns (see Ref. [17]). Resistivity and magnetization for the films were measured in a superconducting magnet with an electrometer and a vibrating sample magnetometer, respectively. For the ISHE measurements, a 10-nm-thick Pt layer was sputtered in an Ar atmosphere on the top of the La_2NiMnO_6 films (4×2 mm^2). The simultaneous measurement of microwave resonance and dc voltage was performed using coplanar-type waveguides [18]. The ISHE measurement at room temperature was conducted by use of an electromagnet, while that at low and high temperatures was carried out in a superconducting magnet with the incident microwave power of 1 W due to a relatively large transmission loss of incident microwave energy [17], the small resonance absorption of La_2NiMnO_6 ($\sim$10 μW), and larger voltage noises at higher temperatures. We applied microwave by means of a signal generator or a vector network analyzer and measured resonance absorption with a microwave power meter. dc voltage generation between the ends of the Pt layer at spin resonance was detected with a nanovoltmeter.

We show x-ray diffraction patterns for our samples in Fig. 2(b). Sharp (002) and (004) diffraction peaks of the La_2NiMnO_6 film were clearly observed, indicating that La_2NiMnO_6 films were epitaxially grown on the (001) STO substrates. The out-of-plane lattice parameter is 3.85 Å, which is almost the same as that of highly ordered films [19,20]. As shown in Fig. 2(b), clear Laue fringes appear around (002) and (004) reflections, indicating high crystalinity, flat surface, and homogeneity of the growth film [21]. From the period of the fringe oscillation, thickness (t) of the La_2NiMnO_6 film was estimated to be 80 nm.

The La_2NiMnO_6 film was confirmed to be highly insulating; sheet resistance R_s is higher than 20 MΩ below 350 K. The high resistance at room temperature enables us to study the spin pumping free from electric conduction in La_2NiMnO_6. Temperature (T) and magnetic field (H) dependence of magnetization (M) is shown in Figs. 2(c) and 2(d), respectively. A clear ferromagnetic-paramagnetic transition is observed at the Curie temperature $T_C \sim 270$ K [Fig. 2(c)], which is almost the same as the bulk value [22]. As shown in Fig. 2(d), the saturation magnetization at 10 K is almost 5 μ_B/f.u. in accordance with the expected value for the ferromagnetic ordering of Ni^{2+} ($S = 1$) and Mn^{4+} ($S = 3/2$) ions. Magnetic-field dependence of M exhibits a ferromagnetic hysteresis behavior below T_C (with a

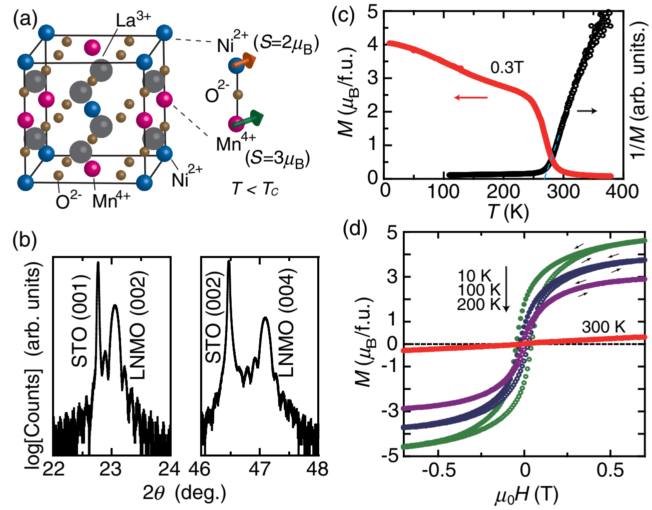

FIG. 2 (color online). (a) Crystal structure of ordered La_2NiMnO_6. Below the critical temperature ($T_C \approx 270$ K), La_2NiMnO_6 exhibits ferromagnetism due to superexchange interaction between Ni^{2+} and Mn^{4+}. (b) $2\theta - \theta$ x-ray diffraction patterns for the 80-nm-thick La_2NiMnO_6 (LNMO) film on the $SrTiO_3$ (STO) substrate. (c) Temperature (T) dependence of magnetization (M) at $\mu_0 H = 0.3$ T for the La_2NiMnO_6 film. T dependence of $1/M$ is also shown in (c). T_C is estimated to be $\sim$270 K from the Curie-Weiss law, where the dotted line is guides to the eyes. (d) Magnetic-field (H) dependence of magnetization (M) at several temperatures.

coercive field of $\sim$50 mT at 10 K). On the other hand, M at 300 K shows linear H dependence, characteristic of the paramagnetic phase [Fig. 2(d)].

The ISHE measurement was performed in both ferromagnetic and paramagnetic states of La_2NiMnO_6, as illustrated in Fig. 1(a), where spin dynamics in the La_2NiMnO_6 was excited by applying a microwave. Here, spin dynamics in a ferromagnetic state is characterized by FMR, while that in a paramagnetic state by electron paramagnetic resonance (EPR). FMR corresponds to a precessional motion of the order parameter—i.e., magnetization—of a ferromagnet. On the other hand, EPR is microwave absorption by individual spin excitation in an external magnetic field [Fig. 1(c)]; when microwave frequency is equal to the magnitude of spin-energy splitting induced by the external magnetic field, transition across the splitting is excited resonantly.

In Fig. 3, we show results of the spin-pumping measurement in a La_2NiMnO_6|Pt device at room temperature, where La_2NiMnO_6 is in the paramagnetic state. Figure 3(a) shows a power spectrum of the microwave reflected from the La_2NiMnO_6|Pt, P, as a function of magnetic field (H) at 300 K. Here, incident microwave frequency (f) and power ($P_{\rm in}$) are $f = 5$ GHz and $P_{\rm in} = 100$ mW, respectively. The power spectrum shows dips around $\pm$0.2 T, which corresponds to microwave absorption by EPR in La_2NiMnO_6. The voltage signal in the Pt layer, V, measured

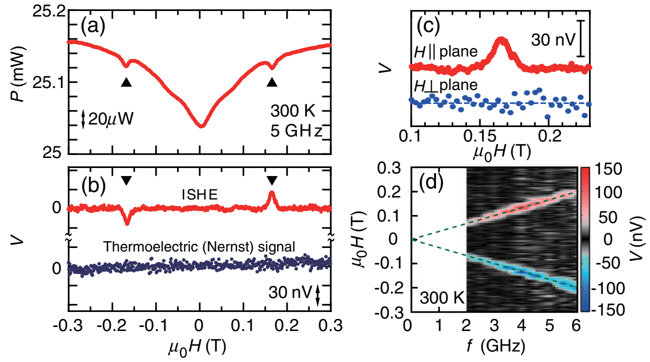

FIG. 3 (color online). (a), (b) Magnetic field (H) dependence of (a) the EPR spectrum (P) and (b) the inverse spin Hall voltage (V) for the La_2NiMnO_6|Pt (10 nm) film. The microwave frequency is kept at 5 GHz and the incident power is 100 mW. The measurement temperature is 300 K. A thermoelectric (Nernst) signal measured under a perpendicular temperature gradient (see text) is shown for comparison in (b); only a tiny normal Nernst signal (with a positive slope) is observed. (c) Comparison of voltage signal (V) between the cases of in-plane H ($H \perp j_s$) and perpendicular-to-plane H ($H \| j_s$). The dotted line is a guide for the eyes. (d) A contour plot of V as functions of frequency (f) and H at 300 K. Incident microwave power (P_{in}) is 0.8 W. The dotted (green) lines are guides for the eyes.

simultaneously with the P measurement is shown as a function of H in Fig. 3(b). At this temperature, the La_2NiMnO_6 is in its paramagnetic phase and there is no long-range spontaneous magnetization. Nevertheless, at the field where EPR occurs, clear electromotive force peaks appear [see Fig. 3(b)]. The La_2NiMnO_6 film is a good insulator whose resistance is larger than 50 MΩ at room temperature, meaning that the voltage signal is generated in the Pt layer. The sign of the voltage peak is reversed by reversing the H direction and the magnitude of the peak increases linearly with microwave power [17]. As shown in Fig. 3(c), we also confirmed that the voltage signal disappears when H is applied along a perpendicular direction to the film plane ($H \| \sigma \| j_s$). These results are consistent with the symmetry of ISHE [$V \| (j_s \times \sigma)$].

To further confirm that the voltage signal appears in the paramagnetic state, we show, in Fig. 3(d), the f dependence of the resonance magnetic field, H_r, determined from the peak positions in the ISHE measurements at 300 K. In FMR, the relation between H_r and the resonance frequency, f_r, is given by the Kittel formula: $2\pi f_r = \gamma\sqrt{\mu_0 H_r(\mu_0 H_r + M_{\mathrm{eff}})}$, where M_{eff} is the effective spontaneous magnetization which also includes surface anisotropy. As shown in Fig. 3(d), f_r dependence of H_r is linear at 300 K, which indicates that $M_{\mathrm{eff}} = 0$, confirming the EPR condition ($2\pi f_r = \gamma\mu_0 H_r$). From the slope value, we estimated γ to be $\gamma = 1.88 \times 10^{11}\ \mathrm{T^{-1}\,s^{-1}}$, which is almost the same as the free electron's gyromagnetic ratio ($\gamma_e = 1.76 \times 10^{11}\ \mathrm{T^{-1}\,s^{-1}}$). This result again demonstrates the spin-current injection from the paramagnetic state.

The observed peak voltage (V_0) at EPR is not due to heating effects induced by microwave resonance absorption. To examine possible contamination of thermoelectric voltage in the Pt layer, we show, in Fig. 3(b), the Nernst-effect signal induced by a temperature gradient externally applied perpendicularly to the film plane. Here, temperature difference was applied with the use of a 1-kΩ-resistance heater attached on the STO substrate, and the applied power = 0.4 W was set to almost the same level as the incident microwave power in the ISHE measurement ($P_{in} = 0.1$–1 W). As shown in Fig. 3(b), the observed thermoelectric signal is proportional to H and its magnitude is very small; this voltage corresponds to the ordinary Nernst effect (see also Ref. [17]). Because the magnitude of the observed electromotive force signal at EPR is much greater than the thermoelectric voltage despite very small resonance-absorption power $\sim 10\ \mu$W, we can safely rule out possible heating-induced effects in the ISHE measurements. The spin-pumping voltage normalized by the resonance absorption, which indicates the efficiency of paramagnetic spin pumping, is $\sim 30\ \mathrm{nV}/10\ \mu\mathrm{W} = 0.003\ \mathrm{V/W}$ at 5 GHz [Figs. 3(a) and 3(b)], which is comparable to that for the FMR spin pumping in the $Y_3Fe_5O_{12}$|Pt bilayers [12].

We show temperature (T) dependence of the voltage signals between 200 and 350 K in Fig. 4(a). Voltage peaks which correspond to the ISHE induced by spin pumping are

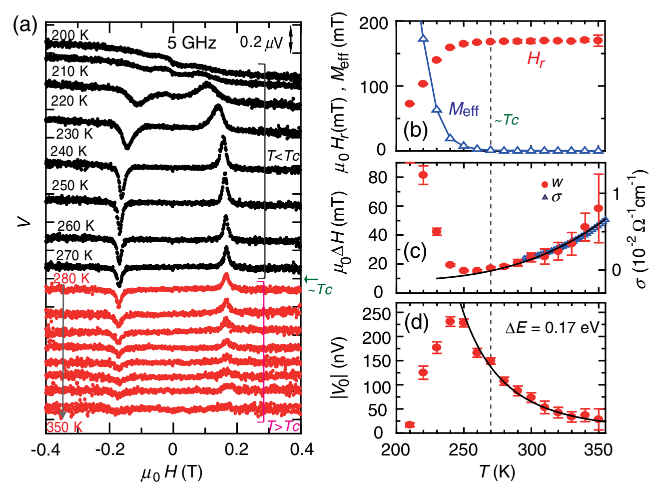

FIG. 4 (color online). (a) Magnetic field (H) dependence of inverse spin Hall voltage (V) at various temperatures. The microwave frequency (f) is 5 GHz. (b) Temperature (T) dependence of the resonance field (H_r) and effective spontaneous magnetization (M_{eff}). The M_{eff} values are estimated using the Kittel formula. (c), (d) Temperature (T) dependence of (c) the full width at half maximum (ΔH) and (d) the magnitude ($|V_0|$) of the peaks in the inverse spin Hall voltage signals. The solid curves in (c) and (d) are fits to Arrhenius equations. Temperature (T) dependence of electrical conductivity (σ) for the La_2NiMnO_6 film is shown for comparison in (c). The dotted vertical lines in (b)–(d) indicate T_C ($\approx$270 K).

observed at each T; it is also noted that small spin Seebeck voltage signals [23] are observed at 200 and 210 K as a broad background, which is asymmetric with respect to H, because of the heating in the waveguide due to microwave energy loss (see also Ref. [17]). Below $T_C \approx 270$ K, the resonance field, or the voltage-peak position H_r, significantly changes with T, while H_r is almost constant above T_C. In Fig. 4(b), $M_{\rm eff}$ values are estimated from the H_r values using the Kittel formula at each T. As T increases from 200 K, the $M_{\rm eff}$ value rapidly decreases and becomes zero above T_C. The temperature dependence of $M_{\rm eff}$ is similar to that of the observed magnetization (M) at 0.3 T shown in Fig. 2(c). The result again confirms that the La_2NiMnO_6 is in its paramagnetic ($M_{\rm eff} = 0$) phase at 300 K where the ISHE signal was clearly observed.

A short-range ferromagnetic correlation above T_C, which was observed in La_2NiMnO_6 [24–27], can be responsible for the persistent spin-pumping signals in such a wide T range above T_C in La_2NiMnO_6|Pt; the short-range correlation was observed above T_C up to 350–400 K, e.g., by Raman spectroscopy [24], and also manifests itself as a small deviation of the inverse susceptibility from the Curie-Weiss behavior above T_C [Fig. 2(c)]. The spin-pumping amplitude is proportional to the two-point correlation function for local magnetization [28], while the static magnetization is proportional to local magnetization itself. Thanks to the short-range correlation, the spin-pumping signal comparable to the ferromagnetic spin pumping is observed even in the paramagnetic state of La_2NiMnO_6. Though such a short-range correlation has been observed also in other ferromagnets above T_C [29,30], the high T_C and strong short-range correlation of La_2NiMnO_6 enable the efficient paramagnetic spin pumping at room temperature.

We fit the ISHE voltage signals around microwave resonance (EPR or FMR) using Lorentz functions and plot the obtained half maximum at full width (ΔH) and peak magnitude $|V_0|$ as a function of T in Figs. 4(c) and 4(d), respectively. As T increases from 200 K, ΔH shows a minimum at 250 K, then increases gradually above T_C [Fig. 4(c)]. On the other hand, the peak voltage $|V_0|$ increases with increasing T from 200 K and shows a maximum at 250 K [Fig. 4(d)]. Above 250 K, $|V_0|$ decreases with increasing T, but it is still prominent even far above T_C up to 350 K [highlighted in red in Fig. 4(a)]. As shown in Figs. 4(c) and 4(d), the overall T dependence of $|V_0|$ is similar to that of the inverse of the linewidth, $1/\Delta H$; the observed enhancement of $|V_0|$ around T_C can be attributed to the suppression of ΔH.

The linewidth ΔH, which reflects the damping for spin precession, exhibits Arrhenius-type T dependence above T_C, as shown in Fig. 4(c): $\Delta H \propto \exp[-\Delta E/k_B T]$. Here, the activation energy ΔE for ΔH is 0.17 eV. We found that this ΔE value is the same as that for the electrical conductivity of the La_2NiMnO_6 film, $\sigma [= 1/(R_s t)]$, as shown in Fig. 4(c). The conductivitylike T dependence of ΔH implies that spin relaxation occurs via thermally excited carriers above T_C. The exponential T dependence of $|V_0|$ ($\propto 1/\Delta H$) above T_C [Fig. 4(d)] shows that the paramagnetic spin pumping is irrelevant to spin waves possibly subsisting above T_C, e.g., paramagnons, which should be related with the T dependence of field-induced magnetization.

As for the lower-T behavior of ΔH ($\sim 1/V_0$), we note that a minimal resonance linewidth and a maximal resonance absorption near T_C such as observed in Figs. 4(c) and 4(d) have been reported in doped perovskite manganese oxides $A_{1-x}A'_x MnO_3$ ($A = $ La, Pr, ...; $A' = $ Ca, Sr, Ba, ...) [31]. For $La_{0.67}Ca_{0.33}MnO_3$ [32] and $La_{0.67}Sr_{0.33}MnO_3$ [33], as T approached T_C from above, the resonance linewidth was reported to go through a minimum and then to increase abruptly below T_C; this is similar to the present case [Fig. 4(c)]. In the previous literature [31,34], the increase in the linewidth below T_C has been attributed to intrinsic magnetic inhomogeneity [31] or a nonuniform demagnetization tensor [34]. Similar effects may cause the increase in ΔH below T_C for the present La_2NiMnO_6 samples.

In summary, we have demonstrated spin pumping above the Curie temperature in a double-perovskite oxide insulator La_2NiMnO_6. The paramagnetic spin pumping in La_2NiMnO_6|Pt which we found operates at room temperature and, in spite of the absence of long-range magnetic order, its efficiency can be comparable to that of typical spin-pumping devices including ferromagnets. Since spin mixing conductance which has been believed to be the language of spin pumping cannot be defined for the paramagnetic state, the paramagnetic spin pumping will require an expansion of the concept of spin pumping.

We thank M. Kawasaki, A. Sawa, and Y. Kajiwara for the experimental help and H. Adachi, D. Hou, R. Iguchi, K. Uchida, and Y. Fujikawa for the fruitful discussions. This work was supported by the CREST "Creation of Nanosystems with Novel Functions through Process Integration" from JST, Grant-in-Aid for Scientific Research A (Grant No. 24244051) from MEXT, the Murata Science Foundation, and the Nippon Sheet Glass Foundation for Materials Science and Engineering.

[1] S. Maekawa, S. O. Valenzuela, E. Saitoh, and T. Kimura, *Spin Current* (Oxford University Press, New York, 2012).

[2] E. Saitoh, M. Ueda, H. Miyajima, and G. Tatara, Appl. Phys. Lett. **88**, 182509 (2006).

[3] M. V. Costache, M. Sladkov, S. M. Watts, C. H. van der Wal, and B. J. van Wees, Phys. Rev. Lett. **97**, 216603 (2006).

[4] A. Azevedo, L. H. Vilela Leão, R. L. Rodríguez-Suárez, A. B. Oliveira, and S. M. Rezende, J. Appl. Phys. **97**, 10C715 (2005).

[5] O. Mosendz, J. E. Pearson, F. Y. Fradin, G. E. W. Bauer, S. D. Bader, and A. Hoffmann, Phys. Rev. Lett. **104**, 046601 (2010).

[6] K. Ando *et al.*, J. Appl. Phys. **109**, 103913 (2011).

[7] A. Azevedo, L. H. Vilela-Leão, R. L. Rodríguez-Suárez, A. F. Lacerda Santos, and S. M. Rezende, Phys. Rev. B **83**, 144402 (2011).

[8] R. H. Silsbee, A. Janossy, and P. Monod, Phys. Rev. B **19**, 4382 (1979).

[9] Y. Kajiwara *et al.*, Nature (London) **464**, 262 (2010).

[10] L. Chen, F. Matsukura, and H. Ohno, Nat. Commun. **4**, 2055 (2013).

[11] C. W. Sandweg, Y. Kajiwara, A. V. Chumak, A. A. Serga, V. I. Vasyuchka, M. B. Jungfleisch, E. Saitoh, and B. Hillebrands, Phys. Rev. Lett. **106**, 216601 (2011).

[12] M. B. Jungfleisch, A. V. Chumak, V. I. Vasyuchka, A. A. Serga, B. Obry, H. Schultheiss, P. A. Beck, A. D. Karenowska, E. Saitoh, and B. Hillebrands, Appl. Phys. Lett. **99**, 182512 (2011).

[13] V. Castel, N. Vlietstra, J. B. Youssef, and B. J. Van Wees, Appl. Phys. Lett. **101**, 132414 (2012).

[14] O. d'Allivy Kelly *et al.*, Appl. Phys. Lett. **103**, 082408 (2013).

[15] H. Nakayama *et al.*, Phys. Rev. Lett. **110**, 206601 (2013).

[16] J. Flipse, F. K. Dejene, D. Wagenaar, G. E. W. Bauer, J. B. Youssef, and B. J. van Wees, Phys. Rev. Lett. **113**, 027601 (2014).

[17] See Supplemental Material at http://link.aps.org/supplemental/10.1103/PhysRevLett.113.266602 for additional data and analysis.

[18] Z. Qiu, T. An, K. Uchida, D. Hou, Y. Shiomi, Y. Fujikawa, and E. Saitoh, Appl. Phys. Lett. **103**, 182404 (2013).

[19] M. Hashisaka, D. Kan, A. Masuno, M. Takano, Y. Shimakawa, T. Terashima, and K. Mibu, Appl. Phys. Lett. **89**, 032504 (2006).

[20] M. Kitamura, I. Ohkubo, M. Kubota, Y. Matsumoto, H. Koinuma, and M. Oshima, Appl. Phys. Lett. **94**, 132506 (2009).

[21] M. Nakamura, Y. Tokunaga, M. Kawasaki, and Y. Tokura, Appl. Phys. Lett. **98**, 082902 (2011).

[22] N. S. Rogado, J. Li, A. W. Sleight, and M. A. Subramanian, Adv. Mater. **17**, 2225 (2005).

[23] K. Uchida, H. Adachi, T. Ota, H. Nakayama, S. Maekawa, and E. Saitoh, Appl. Phys. Lett. **97**, 172505 (2010).

[24] M. N. Iliev, H. Guo, and A. Gupta, Appl. Phys. Lett. **90**, 151914 (2007).

[25] H. Guo, A. Gupta, M. Varela, S. Pennycook, and J. Zhang, Phys. Rev. B **79**, 172402 (2009).

[26] S. Zhou, L. Shi, H. Yang, and J. Zhao, Appl. Phys. Lett. **91**, 172505 (2007).

[27] S. M. Zhou, Y. Q. Guo, J. Y. Zhao, S. Y. Zhao, and L. Shi, Appl. Phys. Lett. **96**, 262507 (2010).

[28] S. Maekawa, H. Adachi, K. Uchida, J. Ieda, and E. Saitoh, J. Phys. Soc. Jpn. **82**, 102002 (2013).

[29] A. P. Li, J. Shen, J. R. Thompson, and H. H. Weitering, Appl. Phys. Lett. **86**, 152507 (2005).

[30] C. He, M. Torija, J. Wu, J. Lynn, H. Zheng, J. Mitchell, and C. Leighton, Phys. Rev. B **76**, 014401 (2007).

[31] J. M. D. Coey, M. Viret, and S. von Molnár, Adv. Phys. **48**, 167 (1999).

[32] S. B. Oseroff, M. Torikachvili, J. Singley, S. Ali, S.-W. Cheong, and S. Schultz, Phys. Rev. B **53**, 6521 (1996).

[33] M. T. Causa *et al.*, Phys. Rev. B **58**, 3233 (1998).

[34] C. A. Ramos, M. T. Causa, M. Tovar, X. Obradors, and S. Piñol, J. Magn. Magn. Mater. **177–181**, 867 (1998).